International Journal of Solids and Structures 163 (2019) 170–177

Contents lists available at ScienceDirect

International Journal of Solids and Structures

journal homepage: www.elsevier.com/locate/ijsolstr

Fracture characteristic analysis of cellular lattice structures under tensile load

Xiaoliang Geng, Yahui Lu*, Chao Liu, Weinan Li, Zhufeng Yue

School of Mechanics, Civil Engineering and Architecture, Northwestern Polytechnical University, Xi'an 710129, PR China

ARTICLE INFO

Article history:
Received 30 October 2018
Revised 3 January 2019
Available online 5 January 2019

Keywords:
Cellular lattice structures
Fracture characteristic
Finite element method
Damage variables
Tensile behavior

ABSTRACT

The fracture characteristic analysis of three-dimensional lattice structures under quasi-static tensile load is explored by finite element method and the simulations are performed with three types of lattice structures: the rhombic dodecahedron and two types of BCC cellular lattice structures with different stacking directions. All the three types of lattice structures are made of ALSi10Mg alloy materials and manufactured using the selective laser melting technique. Also, tensile tests were carried out to obtain mechanical response and failure characteristic of different structures.

This study presents the process of simulation by finite element method and the numerical results predicted with this method reveal novel fracture modes which are consistent with the experimental results respectively: The fracture of the DOD lattice structure is a progressive fracture process which is similar to the crack propagation. For BCC1 and BCC2 lattice structures, the fracture pattern is an entirely rupture along the fracture surface. The differences in the fracture modes of three lattice structures and the evolution processes of damage variables were investigated. In addition, the effects of diameter variation of the struts on the tensile behavior have been observed based on these studies.

© 2019 Elsevier Ltd. All rights reserved.

1. Introduction

Lattice or cellular solids are formed by periodical arrangement of a certain pattern lattice cells, and the struts of lattice cells are straight rods which have regular cell size and shape. Lattice structures have multifarious cell structures and high porosity compared with traditional foam materials (Gergely and Clyne, 2010). It not only has the characteristics of light weight and high specific strength, but also has excellent performance in multi-functional design, such as impact resistance, heat insulation and electromagnetic wave absorption (Boyer, 1996; Kuziak et al., 2008; Xue and Hutchinson, 2004; Kim et al., 2004; Wang et al., 2005; Liu et al., 2007; Yang et al., 2018 2016). However, the lattice structure is difficult to be fabricated with traditional manufacturing methods due to its highly complex spatial structure. The rapid development of additive manufacturing technology in recent years enable the lattice materials being used widely.

Additive manufacturing (AM) technology, such as the Selective Laser Melting technique, is a new type of manufacturing method based on the discrete-cumulative principle. It is a bottom-up approach compared to traditional material removal technologies (Li et al., 2012). This technology allows complex three-dimensional lattice structures to be produced with reducing the time and costs of production (Osakada and Shiomi, 2006; Yan et al., 2012). Mazur et al. (2016) have studied the manufacturing process of SLM technology and the effects of topological configuration, struts dimensions and number of unit cells on structural mechanical properties under compressive load. It was found that SLM technology has the capability to produce complex lattice structure with small geometric defects and excellent performance.

Many scholars have conducted a number of mechanical properties tests by designing diverse lattice structures with different unit configurations and relative densities. The damage characteristics, thermal protection and imperfection of the lattice structure have also been explored. Gibson and Ashby (1999) proposed the concept of a lattice structure and studied the problems of constitutive models and failure modes, etc.; Deshpande et al.'s (2001) research shows that the lattice structure can be simplified to articulated system when the number of struts connected to a node is fixed, meanwhile, the strut is only subjected to axial force and deformation; Alsalla et al. (2016) presented an innovative method for evaluating the local failure mechanism of 316 L stainless steel lattice material under uniaxial tensile and three-point bending load. The results show that the tensile strength and fracture toughness of the lattice structure in different directions are different were obtained. Tserpes and Labeas (2009) explored the tensile behavior of the triangular, hexagonal and Kagome planar lattices containing notches

* Corresponding author.
E-mail address: luyahui@mail.nwpu.edu.cn (Y. Lu).

https://doi.org/10.1016/j.ijsolstr.2019.01.006
0020-7683/© 2019 Elsevier Ltd. All rights reserved.

using FE-based progressive failure analysis. The lattices fail in rupture as an elastic-brittle material is assumed for the struts and the fracture patterns were found to depend only on the topology of the lattices. A dramatic decrease of both stiffness and strength of the lattices with increasing the notch-length were also found in this study. Fleck and Qiu (2007) studied the fracture toughness of elastic-brittle 2D lattices by finite element method for the hexagonal honeycomb, triangular honeycomb and Kagome lattice. The dependence of mode I and mode II fracture toughness upon relative density and the fracture envelope in combined mode I–mode II stress intensity factor space were obtained. The predictions for the tensile and shear strengths of a centre-cracked panel with and analytical estimates were also made. Kucherov and Ryvkin (2012) investigated the flaw nucleation in a brittle open-cell kelvin foam, an initial imperfection was introduced and sequential break of the struts was observed. In addition, different loading directions and material densities were examined and a plane flaw formed by the broken struts was found. Geng et al. (2017) established a finite element model of lattice materials based on combined elements. The combination of solid elements and beam elements improves the computational efficiency while taking the details of stress distribution and deformation characteristics into account. The accuracy and applicability of the modeling method were also verified by comparing with the test results. Although a few studies have addressed the failure mode and mechanical performance of different three-dimensional metallic AM lightweight structures (Mckown et al., 2008). The ductile fracture and propagation of the cracks in the three-dimensional lattice structures are still unclear.

In this context, the present study sought to investigate the failure mechanisms of the three lattice structures manufactured by SLM technology under uniaxial tensile load. Finite element analysis models were established for the three lattice structures, and the simulation results were compared with the experimental results. (Among them, some of the experimental results were obtained by the study of our team's Ma Liyang et al.). The evolutionary process of the damage variables at micro level and effects of diameter variation of the struts on the tensile behavior were also discussed.

2. Materials properties and characteristics of unit cells

The three-dimensional lattice structure is prepared by selective laser melting (SLM) technology, which is a process of melting metal powder under an inert atmosphere by scanning laser continuously and then solidifying them by cooling (Heary et al., 2016). The metal material, AlSi10Mg alloy, is widely used in the aviation field with the advantages of low density, corrosion resistance, etc. Geng et al. (2017) of our research team, have carried out some tensile tests on typical samples fabricated by SLM technology and obtained the fundamental mechanical performance of AlSi10Mg alloy material. The nominal stress-strain curve obtained by the tensile test and the true stress-strain curve modified by the Bridgman (1964)method () are shown in Fig. 1.

In this study, rhombic dodecahedron (DOD) and Body Centered Cubic (BCC) are used as the basic unit cells, in which the rhombic dodecahedron unit cells consist of 12 congruent rhombuses with a total of 32 struts; Body Centered Cubic unit cell is made up of four equilateral triangles with 12 struts in all. Size of this two types unit cells is 4 mm and the nominal diameter of struts is 0.6 mm.

3. Finite element simulation

For the three types of lattice structures, the analysis is performed by means of the Finite Element Method (FEM). For this purpose, the finite element models were established using finite element software ABAQUS/EXPLICIT.

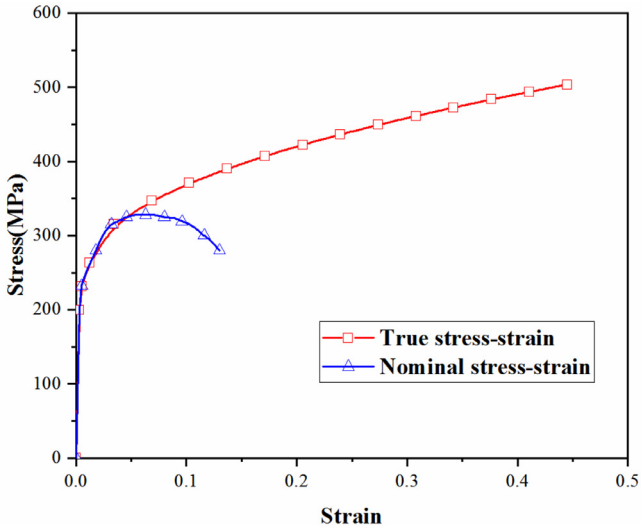


Fig. 1. Stress-strain curve of AlSi10Mg alloy material obtained by tensile test.

3.1. Finite element models

As shown in Fig. 2, three types of the lattice structures are obtained by repeating the various unit cells. Among them, BCC1 and BCC2 have the same unit cell while their stacking directions are perpendicular. The overall size of the structures is 72mm*24mm*24 mm (composed of 6*6*18 cells). In our previous studies (Fleck and Qiu, 2007), the diameter of the struts varies within a range of 0.4–0.8 mm (the given standard diameter is 0.6 mm) due to the limitations of additive manufacturing techniques. Fig. 3 illustrates the SEM photographs of the struts magnified 30 and 100 times, and it can be clearly seen that the strut is not a perfect cylinder (Fleck and Qiu, 2007). Consistent fracture mode was obtained by several sets of experimentations for the lattice structures consisted of the same configuration, and the fracture starts at a defect point or along a flaw surface. Considering this, a thinner strut was taken randomly (except the boundary area) and introduced to the simulation as a tiny imperfect, shown in Fig. 2. Timoshenko beam elements with linear interpolation functions (element type B31 in ABAQUS) are adopted to improve computational efficiency and ensure the accuracy of the simulations (Fleck and Qiu, 2007). All nodes on the bottom side of the lattice structure are constrained in translation and rotation degrees of freedom, and for the upper surfaces of the structures, all translational and rotation degrees of freedom are restricted except the loading direction. Displacement control and smooth analysis steps are imposed to ensure that the simulation is a quasi-static simulation process.

3.2. Material damage initiation and evolution modeling

Generally, two main mechanisms can cause the fracture of a ductile metal: ductile fractures caused by the nucleation, growth and coalescence of void; and shear fractures due to local shear bands formed in the material. These two mechanisms call for two different forms of the criteria, the ductile criterion and the shear criterion, for the onset of damage in ABAQUS (Hooputra and HDell, 2004; ABAQUS 2004).

The ductile criterion assumes that the equivalent plastic strain at the start of damage ε_D^{pl}, is a function of stain rate and stress triaxiality :

$$\varepsilon_D^{pl}(\eta, \dot{\varepsilon}^{pl})$$

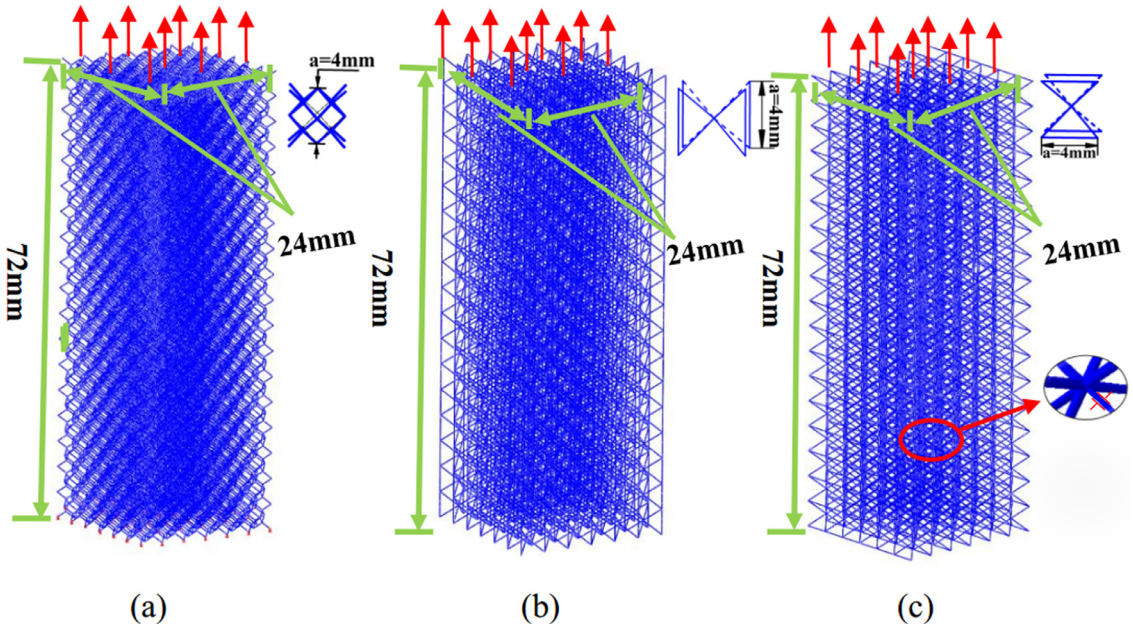


Fig. 2. Finite elements models and unit cells, and each type of lattice structures has a tiny imperfect (labeled with red lines), as shown in the lower right image (a) rhombic dodecahedron (DOD), (b) BCC1 (c) BCC2.

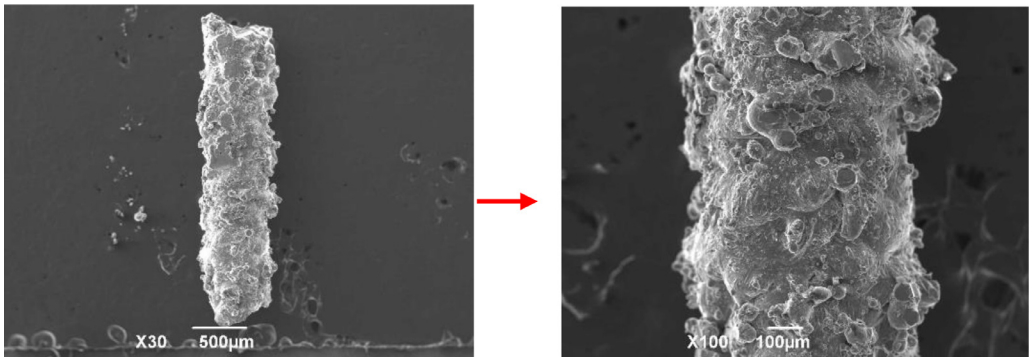


Fig. 3. SEM photographs of a strut magnified 30 and 100 times and non-uniform diameter of the strut can be seen clearly (Geng et al., 2017).

where $\dot{\varepsilon}^{pl}$ is the equivalent strain rate and η is the stress triaxiality. The damage variable, ωD, increases monotonically with plastic deformation and the incremental increase in $\Delta\omega D$ at each increment during the analysis is computed as

$$\Delta\omega D = \frac{\Delta\varepsilon^{pl}}{\varepsilon_D^{pl}(\eta, \dot{\varepsilon}^{pl})} \geq 0$$

And the criterion for damage initiation is met when

$$\omega D = \frac{\Delta\varepsilon^{pl}}{\varepsilon_D^{pl}(\eta, \dot{\varepsilon}^{pl})} = 1,$$

For shear criterion, it's assumed that the equivalent plastic strain at the start of the damage ε_S^{pl} is a function of the shear stress ratio and the strain rate:

$$\varepsilon_S^{pl}(\theta_s, \dot{\varepsilon}^{pl})$$

here $\theta_s = (q + k_s p)/\tau_{max}$ is the shear stress ratio, τ_{max} is the maximum shear stress, and k_s is a material parameter. As the same with ductile criterion, the damage variable, ωS, is proportional to the incremental change in equivalent plastic strain, and the initial damage begins to occur when the following condition is satisfied:.

$$\omega S = \frac{\Delta\varepsilon^{pl}}{\varepsilon_S^{pl}(\theta_s, \dot{\varepsilon}^{pl})} = 1$$

These two damage initiation criterions can be specified for the same material and treated independently. Once a particular initiation criterion is satisfied, the progressive damage of material manifests itself by softening of the yield stress and degradation of the elasticity. Each damage variable,ω_i, have an associated damage evolution law specified in terms of equivalent plastic displacement (Bridgman, 1964). The overall damage variable, D, captures the combined effect of all active mechanisms and is computed in terms of individual damage variables

$$D = \max\{\omega_{mult}, \max(\omega_i)\}$$

Where ω_{mult} is computed by some of the damage variables in a multiplicative sense.

$$\omega_{mult} = 1 - \prod_{i=2}(1 - \omega_i)$$

The material become fails and the "element kill" algorithm available in ABAQUS can be used to delete the failure elements from the mesh when the overall damage variable reaches the value $D = 1$.

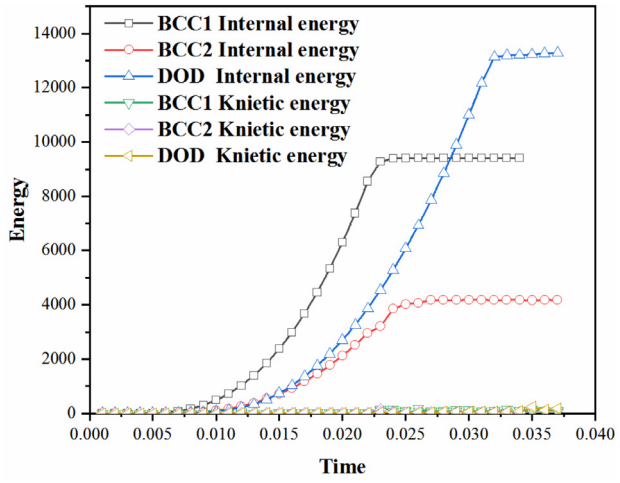


Fig. 4. Energy history diagram in the fracture simulations of three types lattice structure.

3.3. Quasi-static process simulation by ABAQUS/explicit

In our tensile test, the loading rate is 1 mm/min and it can be regard as a quasi-static procedure. The influence of inertial forces should be considered and large plastic deformation with final rupture should be predicted in the simulation. In ABAQUS/Standard module, it is difficult to overcome the non-convergence problem caused by excessive plastic deformation of the elements. The fracture and failure issues should be analyzed by ABAQUS/Explicit module, and it has been proved to be effective in simulating quasi-static loading conditions (Heary et al., 2016). It is necessary to minimize the effects of inertial forces for the quasi-static simulation process, and studying the various energies in the model is an efficient way to assess whether the correct quasi-static response has been generated. The energy balance equation in ABAQUS/Explicit can be expressed as

$$E_I + E_V + E_{KE} + E_{FD} - E_W = E_{total} = \text{Constant}$$

Where *EI* is the internal energy, *EV* is the energy absorbed by viscous dissipation, *EKE* is the kinetic energy, *EFD* is the energy absorbed by frictional dissipation, *EW* is the work done by external force, and *Etotal* is the total energy in the system. In the quasi-static loading simulation of the structure, the inertial force will be negligible and the work done by the external force should be identical to internal energy as much as possible. Moreover, as a general rule, it is acceptable that the kinetic energy of the deformed material will not exceed a small proportion (5% to 10%) of its internal energy (Bridgman, 1964).

The energy history diagram in the simulation processes are plotted in Fig. 4. It can be seen that the kinetic energy of the deformed material is much lower than the internal energy, that is, the simulations are quasi-static stretching processes. In addition, although the BCC1 lattice structure has the highest carrying capacity, the DOD lattice structure has the greatest internal energy because of its large structural deformation. For BCC1 and BCC2 lattice structures with the same unit cell, the BCC2 lattice structure has the lowest internal energy, indicating that it has the weakest bearing capacity. More details will be expressed below.

4. Results and discussion

The quasi-static stretching process of the three types lattice structures were simulated through the above introduced methods. Unexpected fracture patterns that are consistent with the test results were found from the simulations. Damage evolution of the three types lattice structures were analyzed. In addition, effects of different radius of the struts on the tensile mechanical properties were discussed.

4.1. Macroscopic fracture analysis of three types lattice structures

Fig. 5 illustrates the macroscopic morphology of fracture surfaces obtained by experiments and simulations, which are coincident with each other respectively. As can be seen from the picture, the fracture section of DOD lattice structure has a rhombic shape; the fracture sections of the BCC1 and BCC2 are inclined by about 45° and 30° to the load direction correspondingly.

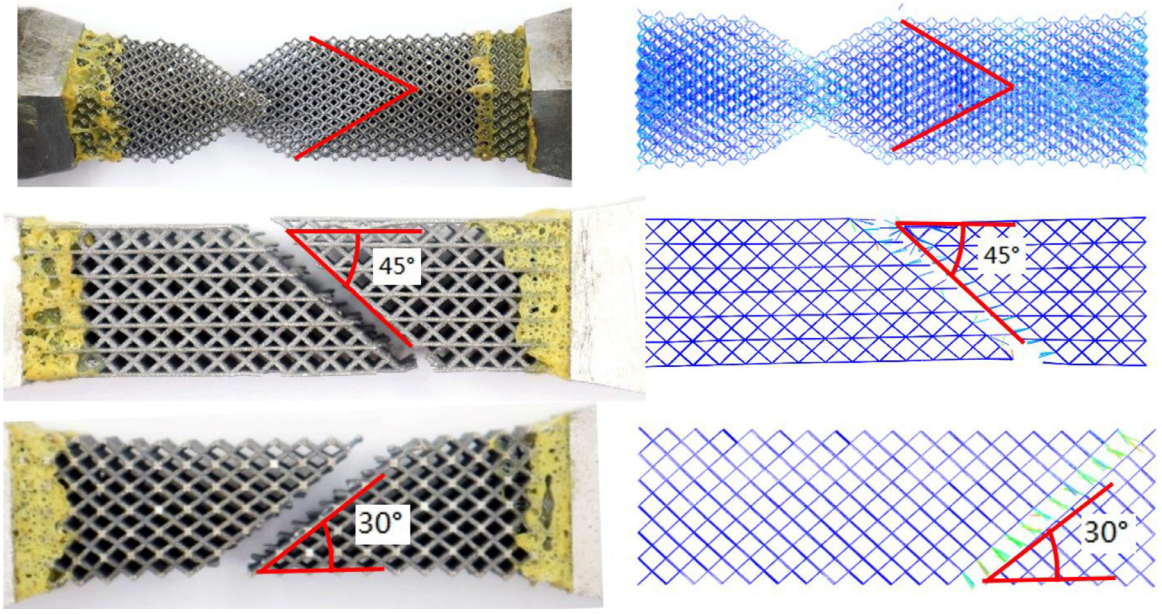


Fig. 5. The macroscopic morphology of fracture surface obtained by experiments and simulations (a) DOD (b) BCC1 (c) BCC2.

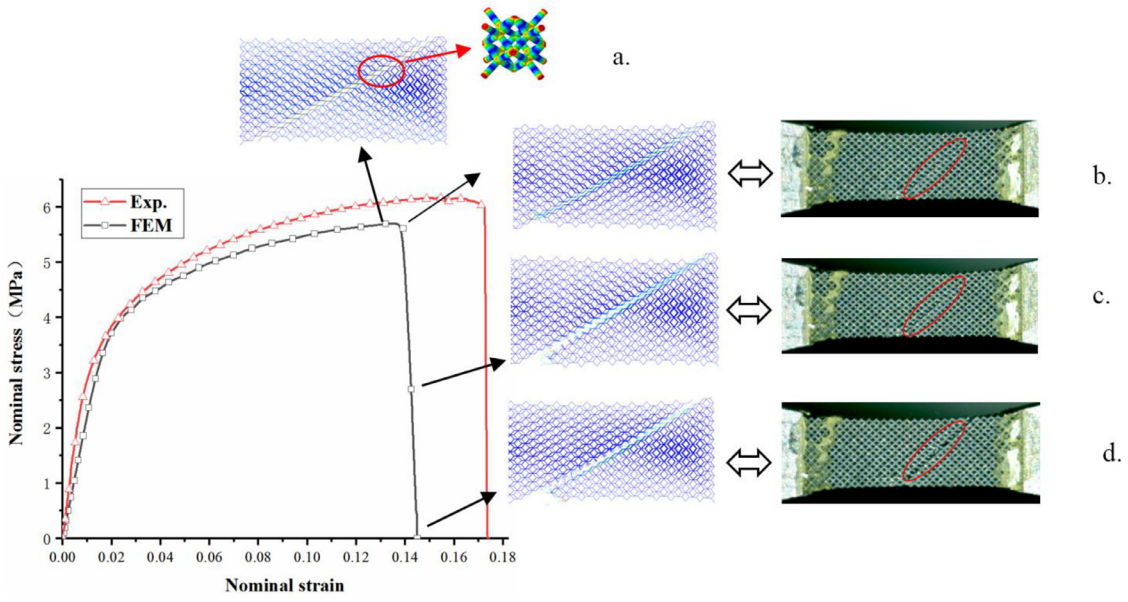


Fig. 6. Nominal stress–strain curves and fracture progression of the BOD lattice structure under the tensile load obtained by FEM and experiment (a) The "slip" of the struts; (b) Initial fracture point near the defect formation; (c) The "crack" develop along the fracture surface; (d) Overall fracture of the lattice structure.

4.1.1. Fracture process of the DOD lattice structure

Fig. 6 shows nominal stress-strain curves and deformation process of the DOD lattice structure under the tensile load obtained by FEM and experiment. It can be drawn that the ultimate strength and strain obtained by the simulation are less than the experimental results. The strain measurement in the test was performed using a non-contact video extensometer, which collects data by tracking marks on the test samples. The deviations between the test and simulation results may be caused by the non-uniform diameter of the struts. In addition, it should be noted that for the convenience of observation, the model in the simulation picture was rotated at a certain angle. The fracture process of the DOD lattice structure mainly includes three phases: the "slip" of the struts; initial fracture point formed near the defect and develop along the fracture surface similar to crack propagation. High-speed camera was also used to capture the details of the fracture process in the experiment, unfortunately, because the procedure is extremely rapid, only a few fragments were observed.

A number of unit cells were taken along the fracture surface for analysis. It can be found that the maximum stress is concentrated at corners. As the displacement increase constantly, the cross struts began to rotate, initial damage occurred at the corners and gradually evolved until the element was deleted eventually. The images in Fig. 7 illustrates the damage variables versus the true strain of the element. DUCCRT is the state variable (ωD) that characterizes the ductile criterion, SHRCRT is the state variable (ωS) that characterizes the shear criterion, DMICRT is the overall damage variable (D) and it's coincide with the ductile variable (ωD) exactly. It can be concluded that the generation and evolution of the initial damage of the struts in the DOD unit cells follows the ductile criterion, which means that the ductile fracture caused by the nucleation, growth and coalescence of void are dominant.

4.1.2. BCC1 and BCC2 lattice structures

The BCC1 and BCC2 lattice structures are stacked in different directions with the same unit cell configuration. Neither of them appears as a process in which a crack propagates along the fracture surface as DOD lattice structure, but breaks directly after the "slip" of the struts at the dangerous section. As depicted in Fig. 8, the nominal strain of the BCC1 lattice structure obtained by the

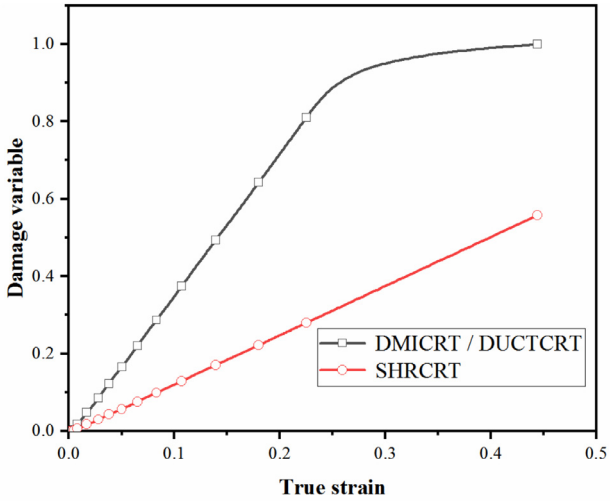


Fig. 7. Damage variable vs. element true strain for DOD lattice structure under quasi-static stretching process.

simulation is less than the test, and the ultimate strengths are almost equal to each other. Other than that, two adjacent unit cells at the fracture surface were taken, and it can be observed that the fracture process of BCC1 lattice structure can be divided into two stages (It's a pity that the extremely rapid fracture process of the BCC lattice structures was still not captured clearly although the high-speed camera was used for the test):

Firstly: the axial struts as the main bearing components with higher stress, large plastic deformation and initial damage occurs in them. As the displacement increases, the damage continues to develop until the element was removed, with the axial struts breaks.

Secondly: the cross struts of the unit cell began to be the dominant bearing member and rotates around the cross point after the axial struts breaks. Then, initial damage occurs at corners and continues to evolve until the unit was deleted, meanwhile, the BCC1 lattice structure achieved overall fracture.

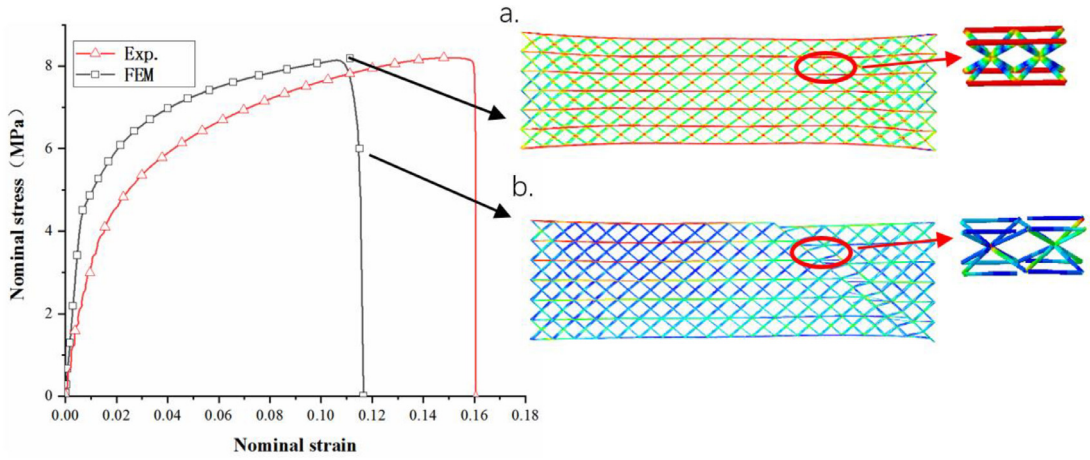


Fig. 8. Comparison of nominal stress–strain curves for BCC1 lattice structure and two stages of the fracture process: (a) Deformation of the structure and the axial struts as the main bearing components; (b) Axial struts break and "Slip" of the cross struts.

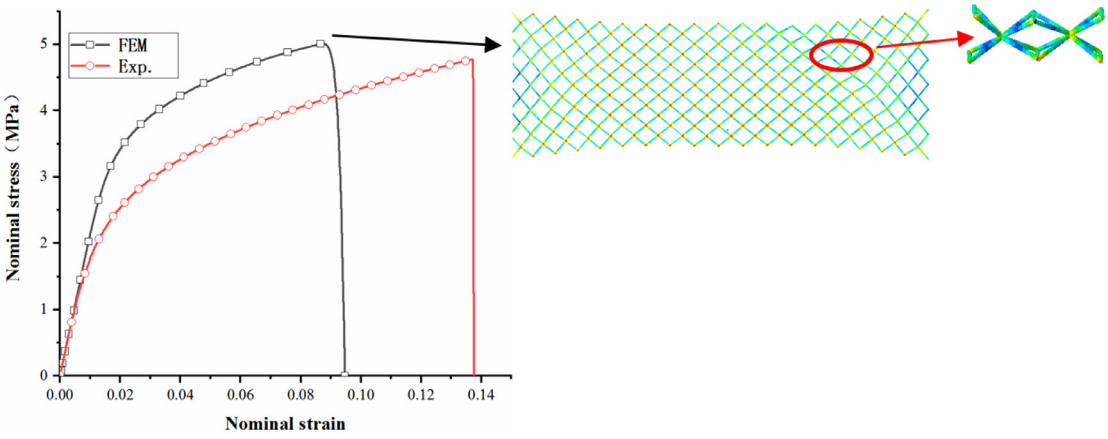


Fig. 9. Nominal stress–strain curves obtained by experiment and simulation and fracture progression of the BCC2 lattice structure.

Compared with the BCC1 and DOD lattice structures, the BCC2 lattice structure has a simple fracture process: with the displacement increases, the cross struts of the unit cell undergo the bending moment and the tensile load. Initial damage occurs at corners and continues to growth. Finally, the elements are deleted and the BCC2 lattice structure is overall broken simultaneously. Fig. 9 exhibits the fracture process and comparison of nominal stress-strain curves of the BCC2 lattice structure under the tensile load.

For the BCC1 and BCC2 lattice structures, both criteria for the initial damage generation and evolution are triggered. The damage variables as a function of the strain are identical to each other, as seen in Fig. 10.

In summary, we can find that the fracture process of the DOD lattice structure is a progressive fracture evolution which is similar to the crack propagation, while for the BCC1 and BCC2 lattice structures, the fracture pattern begins with the formation of an dangerous cross-section and the subsequent entirely fracture along it. In addition, it can be seen that the BCC1 and BCC2 lattice structures have the same unit cell configuration, and the dominant criteria in the damage are consistent with each other but different from the DOD lattice structure. Therefore, we can conclude that the unit cell configuration determines the fracture mode of the lattice structure and make the following suppositions: the lattice structures consisting of the same type of the unit cell may have the identical damage initiation criterion and for structures with different types of the unit cells, analyzing their corresponding unit cells may be a good way to evaluate the mechanical properties.

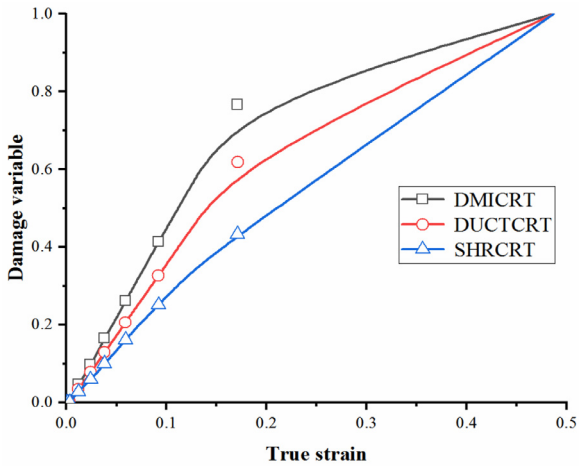


Fig. 10. Damage variable strain curve of BCC1 and BCC2 lattice structures under quasi-static stretching process.

4.2. Effects of diameter of the struts on the mechanical behavior of three types lattice structures

As shown in Fig. 3, the diameter of the strut is randomly distributed within a range and the impacts of this issue on mechanical properties of lattice structure is still unclear. This question is

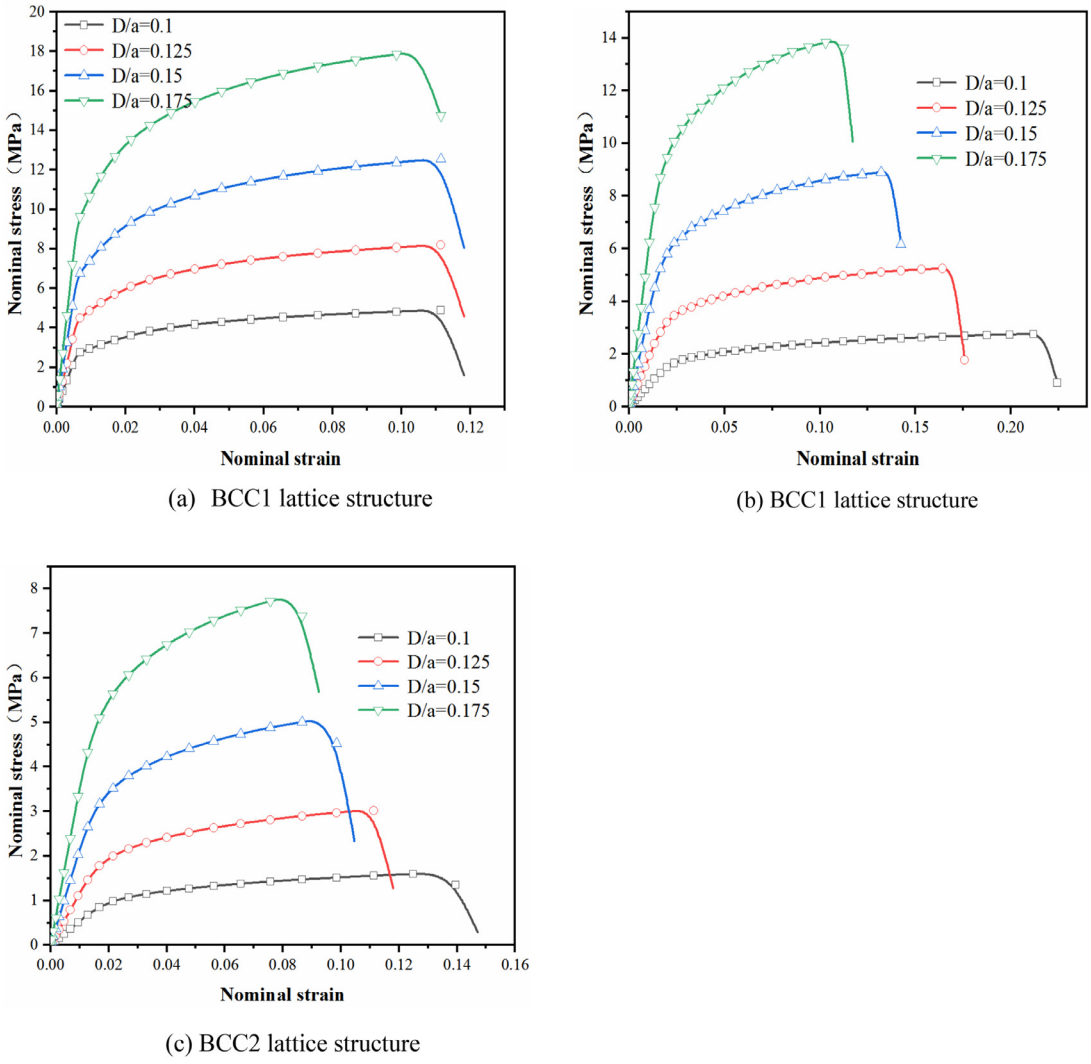


Fig. 11. Comparison between the nominal stress-strain curves of the lattices with different ratios of diameter to unit cell size.

complex and will be explored in our future study. But through current investigation, we can give the upper and lower limits of the structural strength, which is also the concern of the application. Furthermore, the influence of the diameter variation of the struts on mechanical properties of the lattice structure should be known to the designer in the engineering application. However, it is difficult to obtain the results by theoretical calculation because of the highly complex spatial structural characteristics. Consequently, this issue was addressed by the method described above and the nominal stress-strain curves of three types lattice structures at different ratios of diameter to unit cell size (D/a) are plotted in Fig. 11. Here, the unit cell size is a fixed value, $a = 4$ mm, as described above.

As expected, the diameter variation of the struts has significant effects on the tensile mechanical properties of the lattice structures. The tensile strength of the structure increases with increasing diameter of the strut, and the trend of the BCC2 is more slow compared with the BCC1 and DOD lattice structures, as shown in Fig. 12. The variation of diameter has little effect on ductility of the BCC2 lattice structure while correlated with the ductility negatively for BCC1 and DOD lattice structures. Fig. 13 indicates that the diameter of the strut has a significant positive correlation with the stiffness of the BCC1 structure, but has little effect on BCC2 and DOD lattice structures. Both BCC2 and DOD lattice structure

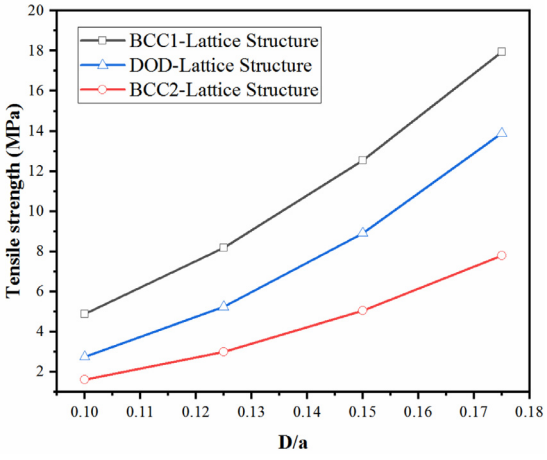


Fig. 12. Tensile strength of the lattices structures with respect to varies ratios of diameter to unit cell size.

have low stiffness, as a result of the BCC2 lattice structure has low carrying capacity, while the DOD lattice structure has a better ductility.

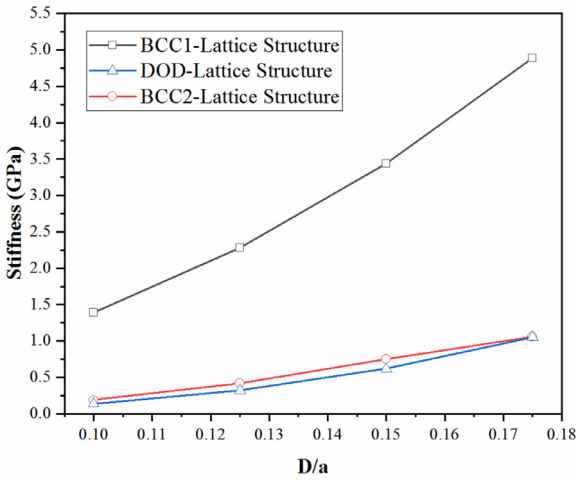


Fig. 13. Stiffness of the lattices structures with respect to varies ratios of diameter to unit cell size.

5. Conclusion

In this paper, the fracture patterns of three types lattice structures are simulated by the finite element method, and the predicted simulation using this method are consistent with the test results. The differences in the fracture modes of three types lattice structures and the evolution processes of the damage variables were investigated. Also, the influence of diameter variation on the tensile behavior of the three types lattice structures were also analyzed. From the above studies, the following conclusions are drawn:

1. The type of unit cell configuration determines the fracture mode of the lattice structure. The fracture process of the DOD lattice structure is a progressive fracture evolution which is similar to the crack propagation, while for the BCC1 and BCC2 lattice structures, the fracture begins with the formation of an entirely fracture surface and the subsequent fracture of it.
2. The generation and evolution of the initial damage of the struts in the DOD unit cells follows the ductile criterion, that is, the ductile fracture caused by the nucleation, growth and coalescence of void are dominant. The lattice structures obtained from the same unit cell configuration (BCC1 and BCC2) have the identical initial damage generation criterion and evolution process.
3. The tensile strength of the structure increases with increasing diameter of the struts, and the increasing trend of the BCC2 lattice structure is more slow compared with the BCC1 and DOD lattice structures. The diameter of the strut has a significant positive correlation with the stiffness of the BCC1 structure, while has little effect on BCC2 and DOD lattice structures.

Acknowledgement

This study is supported by the Aeronautical Science Foundation of China (No: ASFC-20170153001).

References

ABAQUS, 2004. ABAQUS/Explicit User's Manual Version 6.14. ABAQUS Inc.
Alsalla, H., Liang, H., Smith, C., 2016. Fracture toughness and tensile strength of 316 L stainless steel cellular lattice structures manufactured using the selective laser melting technique. Mater. Sci. Eng. A 669, 1–6.
Boyer, R.R., 1996. An overview on the use of titanium in the aerospace industry [J]. Mater. Sci. Eng. A 213, 103–114.
Bridgman, P.W., 1964. Studies in Large Plastic Flow and Fracture. Harvard University Press.
Deshpande, V.S., Ashby, M.F., Fleck, N.A., 2001. Foam topology: bending versus stretching dominated architectures. Acta Mater. 49, 1035–1040.
Fleck, N.A., Qiu, X.M., 2007. The damage tolerance of elastic–brittle, two-dimensional isotropic lattices. J. Mech. Phys. Solids 55, 562–588.
Geng, X., Ma, L., Liu, C., et al., 2017. A FEM study on mechanical behavior of cellular lattice materials based on combined elements. Mater. Sci. Eng. A. 712, 188–198.
Gergely, V., Clyne, B., 2010. The FORMGRIP process: foaming of reinforced metals by gas release in precursors. Adv. Eng. Mater. 2, 175–178.
Gibson, L.J., Ashby, M.F., 1999. Cellular solids: structure and properties. Cambridge University Press.
Heary, M., Mazur, M., Elambasseril, J., et al., 2016. Selective laser melting (SLM) of AlSi12Mg lattice structures. Mater. Des. 98, 344–357.
Hooputra, HGese, HDell, et al., 2004. A comprehensive failure model for crashworthiness simulation of aluminium extrusions. Int. J. Crashworthiness 9, 449–464.
Kim, T., Hodson, H.P., Lu, T.J., 2004. Fluid-flow and end wall heat-transfer characteristics of an ultralight lattice-frame material. Int. J. Heat Mass Transf. 47, 1129–1140.
Kucherov, L., Ryvkin, M., 2012. Flaw nucleation in a brittle open-cell Kelvin foam. Int. J. Fract. 175, 79–86.
Kuziak, R., Kawalla, R., Waengler, S., 2008. Advanced high strength steels for automotive industry. Arch. Civ. Mech. Eng. 8, 103–117.
Li, D., Tian, X., Wang, Y., & Lu, B. 2012. Developments of additive manufacturing technology. Electromachining Mould.
Liu, T., Deng, Z.C., Lu, T.J., 2007. Bifunctional optimization of actively cooled, pressurized hollow sandwich cylinders with prismatic cores. J. Mech. Phys. Solids 55, 2565–2602.
Mazur, M., Leary, M., Sun, S., et al., 2016. Deformation and failure behaviour of Ti-6Al-4 V lattice structures manufactured by selective laser melting (SLM) [J]. Int. J. Adv. Manuf. Technol. 84, 1391–1411.
Mckown, S., Shen, Y., Brookes, W.K., et al., 2008. The quasi-static and blast loading response of lattice structures. Int. J. Impact Eng. 35, 795–810.
Osakada, K., Shiomi, M., 2006. Flexible manufacturing of metallic products by selective laser melting of powder. Int. J. Mach. Tools Manuf. 46, 1188–1193.
Tserpes, K.I., Labeas, G.N., 2009. Progressive fracture analysis of planar lattices and shape-morphing Kagome-structure. Theo. Appl. Fract. Mech. 51, 41–47.
Wang, J., Lu, T.J., Woodhouse, J., Langley, R.S., Evans, J., 2005. Sound transmission through lightweight double-leaf partitions: theoretical modelling. J. Sound Vib. 286, 817–847.
Xue, Z., Hutchinson, J.W., 2004. A comparative study of impulse-resistant metal sandwich plates. Int. J. Impact Eng. 30, 1283–1305.
Yan, C., Liang, H., Raymont, D., 2012. Evaluations of cellular lattice structures manufactured using selective laser melting. Int. J. Mach. Tools Manuf. 62, 32–38.
Yang, W., Liu, Q., Gao, Z., et al., 2018. Theoretical search for heterogeneously architected 2D structures. Proc. Natl. Acad. Sci. 115, E7245–E7254.
Yang, W., Yue, Z., Xu, B., 2016. A hybrid elastomeric foam-core/solid-shell spherical structure for enhanced energy absorption performance. Int. J. Solids Struct. 92, 17–28.